

# A Non-Foster Superconducting Broadband Matching Network

A. K. Yi,<sup>1,2</sup> P. Stark,<sup>3</sup> and C. Bartram<sup>1,2</sup>

<sup>1</sup>*SLAC National Accelerator Laboratory, 2575 Sand Hill Road, Menlo Park, California 94025, USA*

<sup>2</sup>*Kavli Institute for Particle Astrophysics and Cosmology, Stanford University, 452 Lomita Mall, Stanford, CA, 94305, USA*

<sup>3</sup>*Department of Physics, Stanford University, 382 Via Pueblo Mall, Stanford, CA, 94305, USA*

(Dated: 12 March 2026)

The nonlinear inductance of the Josephson junction has enabled the development of a wide range of continuous-variable amplifiers and qubit-based devices with unprecedented sensitivity. We present an alternative use of the Josephson junction in the context of broadband impedance matching. The idea poses a potential solution to a longstanding problem in the field of high energy particle physics. The axion, a compelling candidate for the dark matter, converts to a weak electromagnetic signal at an as-yet unknown frequency. As such, the ideal axion detector does not compromise bandwidth for sensitivity, a trade-off intrinsic to all linear, time-invariant and passive circuits. We propose a circuit that uses a Josephson junction in an impedance matching network to overcome these gain-bandwidth constraints and increase the scan rate of axion searches. The Josephson junction can be biased to exhibit negative inductance capable of canceling geometric inductance similar to a capacitor but across a wider frequency range.

## I. INTRODUCTION

### A. Motivation

Broadband impedance matching is an important area of research within antenna, microwave, and radio frequency (RF) engineering<sup>1-3</sup>. Impedance matching is a fundamental design consideration in network analysis to minimize signal loss due to internal reflection, thus maximizing transfer efficiency between a signal source and load. However, a classical impedance-matched complex network can only achieve optimal matching over a finite bandwidth.

This limitation is described by the Bode-Fano limits, which constrain the average value of the inverse magnitude of the reflection coefficient as a function of frequency for classical passive, linear, and time invariant (LTI) networks with complex loads<sup>4,5</sup>. This gain-bandwidth product imposes stringent constraints on the design of broadband matching networks, and considerable efforts have been dedicated to developing network architectures that present bandwidth improvements over this classical limit.

Evading the Bode-Fano limits can be done through the use of *non-Foster* networks, which incorporate active devices that violate the Foster reactance theorem and subvert the passive LTI assumptions behind the Bode-Fano limits<sup>6</sup>. These networks are often realized as active semiconductor-based circuits with negative impedances, such as negative impedance converters (NICs) constructed out of operational amplifiers<sup>7-10</sup>.

Historical approaches to Bode-Fano evasion using non-Foster elements have especially focused on high quality factor (high- $Q$ ) networks

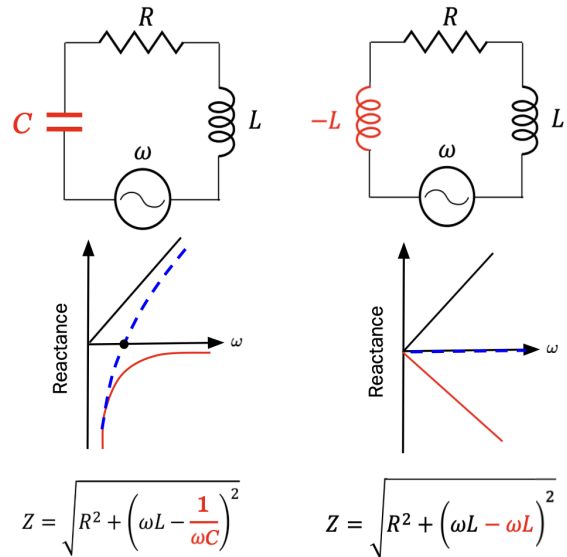


FIG. 1: Left: In a classical, single-pole resonant matching network, the reactive impedance is canceled at a single value, indicated by the zero crossing of the total reactive inductance. Right: In a non-Foster network with idealized negative inductance instead of capacitance, the reactive impedance is instead canceled across all frequencies, resulting in a technically infinite bandwidth network.

within the radio and microwave frequency band. These systems tend to be dominated by reactive impedances, rather than radiative losses, which leads to a narrowband network where the impedance is only perfectly matched at a single *resonant* frequency. In contrast, an ideal non-Foster network with a negative reactive impedance

could cancel the reactance at *all* frequencies, resulting in an infinite bandwidth device, as shown in Fig. 1. Existing applications of non-Foster networks at these frequencies include the development of electrically small antennas for broadband communication and imaging<sup>11–15</sup>, dispersion compensation in active metamaterial and 2D structures<sup>16–18</sup>, high power transmission line design<sup>19,20</sup>, fast-wave propagation<sup>21</sup> and superluminal waveguides<sup>22</sup>.

A newfound driver in the development of non-Foster networks arises in the field of high energy particle physics. A compelling dark matter candidate known as the axion is predicted to convert to an electromagnetic signal in a magnetic field<sup>23</sup>. The axion of quantum chromodynamics, or QCD axion, is thought to be highly motivated due to its ability to simultaneously explain a related problem in high energy physics<sup>24–30</sup>. Once thought too weak to detect, signals of the requisite strength for the QCD axion were first rendered visible through the combination of a high- $Q$  resonator and SQUID amplifier<sup>31,32</sup>. Nevertheless, this circuit’s necessarily high quality factor imposes strict limits on its bandwidth in accordance with the Bode-Fano constraints. As such, coverage of the full parameter space proceeds at an excruciatingly slow pace, with estimates of required scan time at tens of thousands of years<sup>33</sup>.

The concept of improved impedance matching to the dark matter has been discussed in general terms, but, to our awareness, no specific implementation along these lines has been proposed. In analogy to the bandwidth limitations on passive LTI matching networks, a rigorous derivation on the fundamental limitations to the scan rate of axion searches has been developed<sup>34,35</sup>. In contrast, in this work, we present a circuit design that is no longer limited by the aforementioned bandwidth constraints. One requirement in the search for the axion is the maintenance of the extraordinary sensitivity achieved through the use of cryogenic superconducting materials. We propose a technique that fulfills this requirement while achieving a match over a wider bandwidth than that of a passive, LTI circuit. Our technique leverages the nonlinear, negative inductance of the Josephson junction as part of the impedance matching network that functions as the axion detector.

The Josephson junction is a cryogenically operated active device that consists of two superconductors interrupted by an insulating barrier. When a bias current smaller than the critical current of the junction is applied, the device exhibits Cooper pair tunneling across the insulator, inducing a non-dissipative supercurrent related to the phase difference between the superconducting regions. The effective inductance of the Josephson

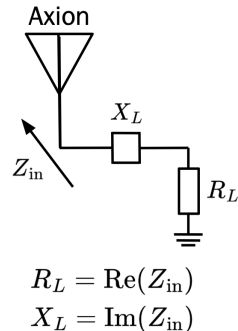


FIG. 2: Load receiver model for a signal with a complex source impedance. For a detector to achieve a perfect match, the real impedance of the ‘load’ (the readout) must match the real component of the source impedance, while the complex load impedance must equal the complex conjugate of the complex source impedance.

junction can be written as

$$L_J(\phi) = \frac{\Phi_0}{2\pi I_c \cos \phi} = \frac{L_{J,0}}{\cos \phi}, \quad (1)$$

where  $\phi$  is the phase across the junction,  $I_c$  is the critical current of the junction, and  $\Phi_0$  is the magnetic flux quantum. This sinusoidal relationship implies that inductance across the junction takes on negative values for  $\pi/2 < \phi < 3\pi/2$ . Previous works have demonstrated this inductance-phase relation and discussed the negative inductance regime, but not in the context of broadband impedance matching<sup>36,37</sup>.

## II. CIRCUIT DESIGN

In this section, we introduce a Josephson junction-based circuit design that achieves negative inductance as part of a non-Foster device. The proposed device is intended to serve as a novel matching network between a complex-valued source impedance and the signal readout (Fig. 2). This model is especially relevant in the context of lumped element axion searches, which operate in a regime where the primary observable for the axion is a dark matter-induced magnetic field. Under these assumptions, the signal arising from the axion dark matter can be modeled as a perfectly stiff AC voltage source. Axion detectors operating under these conditions can couple inductively to this signal, which introduces a complex term to the source impedance that must be matched by the network to maximize the transfer of signal power incident on the pickup to the readout.

If the source impedance is predominantly inductive, then the most efficient narrowband match is a capacitor, canceling the pickup inductance at a

single frequency. We propose to replace the capacitor with a Josephson junction-based device, acting as a non-Foster component to cancel the geometric inductance. In Sections II A and II B, we derive the analytic expression for the total effective inductance and discuss the choice of circuit parameters needed to achieve effective negative inductance. In subsequent sections, we simulate and compare the power transfer within our matching network to that of the classical resonant match. Finally, we discuss the noise and stability for the proposed device, as well as the implications for its use in an axion search.

### A. Flux quantization in a superconducting loop

To understand the operating principle of a potential non-Foster device, we first consider a simple example of a flux-biased superconducting loop interrupted by a Josephson junction (Fig. 3). We explicitly denote the geometric inductance of the loop as an inductance  $L_G$  and ignore dissipative effects aside from those present in the junction model.

If the loop is threaded with an external flux  $\Phi_{\text{ext}}$ , a current is induced within the loop according to the first Josephson equation. Taking into account the loop inductance, the total flux in the loop is given by

$$\Phi = \Phi_{\text{ext}} + L_G I = \Phi_{\text{ext}} - L_G I_c \sin(2\pi\Phi/\Phi_0), \quad (2)$$

where  $I$  is the current induced in the loop and  $\Phi_0$  is the magnetic flux quantum. We also impose periodic boundary conditions on the phase and substitute the current in terms of the critical current of the junction,  $I_c$ . We make one final substitution by substituting the reduced junction inductance,  $L_{J,0}$ , for the current:

$$\Phi = \Phi_{\text{ext}} - \frac{L_G}{L_{J,0}} \frac{\Phi_0}{2\pi} \sin(2\pi\Phi/\Phi_0). \quad (3)$$

The above equation can be expressed in terms of the phase across the junction,  $\phi$ , as

$$\frac{\Phi_0}{2\pi} \left[ \phi - \phi_0 + \frac{L_G}{L_{J,0}} \sin \phi \right] = n\Phi_0, \quad (4)$$

where  $L_G$  is the geometric inductance associated with the inductor,  $n$  is an integer imposing flux quantization, and  $\phi_0$  is the external phase bias associated with external applied flux  $\Phi_{\text{ext}} = (\Phi_0/2\pi)\phi_0$ .

The ratio of  $L_G/L_{J,0}$  is the inductance parameter,  $\beta_L$ , which is related to the ratio  $E_L/E_J$  and determines whether the above expression is single-valued (non-hysteretic) or multi-valued. To use the junction as a non-Foster device, the junction must be in the negative inductance regime. This corresponds to a junction phase  $\pi/2 < \phi < 3\pi/2$ ,

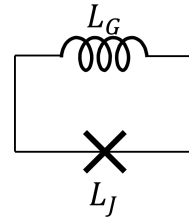


FIG. 3: A superconducting circuit loop with a geometric inductance, whose value is denoted by  $L_G$ , and Josephson junction with inductance  $L_J$ .

with the maximum value among negative inductances occurring at  $\phi = \pi$ . For the rest of the discussion, we will use  $\pi$  as the optimal phase bias point for maximal impedance matching. In non-hysteretic ( $\beta_L < 1$ ) operation, Eq. 4 is single-valued and yields a junction phase  $\pi$  when the external flux bias is set to  $\pi$ . Note that this choice of optimal bias point only holds for non-hysteretic operation.

### B. Extended Circuit Diagram

In Sec. II A, we established that the junction can be directly biased into the negative inductance regime through the external phase bias as long as the geometric inductance seen by the junction is smaller than the reduced junction inductance,  $L_{J,0}$ . The proposed device (pictured in Fig. 4) expands on the above principle to incorporate the junction into a generalized AC matching network. The device is now coupled to a broader network and its input port now includes its inductive coupling to the rest of the detector.

We initially bias the junction to phase  $\pi$  to prepare the negative inductance state. The junction loop is then strongly coupled to the pickup loop that represents the inductive pickup of our axion or other radio-frequency signal detector.

For the junction to remain non-dissipative, we assume that the applied drive voltage only creates currents across the junction that are much smaller than its critical current. When an RF signal appears on the input of the device, an AC component is introduced to the induced current within the junction loop. For sufficiently small signals, the phase across the junction,  $\phi(t)$ , gains a small time-dependence, but remains biased to a phase very close to  $\pi$ . In that case, the dynamical behavior of the junction is described by the ‘tilted washboard potential’ with a tilt that restricts the phase to small oscillations about a local minimum<sup>38</sup>.

In this small phase-limit of the junction (where the phase excursions are small), the junction acquires the effective inductance introduced in Eq. 1. For an arbitrary coupling coefficient  $k$ , the effec-

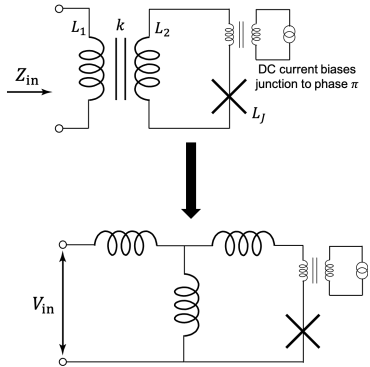


FIG. 4: Proposed non-Foster junction device with its equivalent circuit representation. The Thevenin equivalent look-back impedance at that port is  $Z_{in}$ , with a corresponding voltage  $V_{in}$  across the terminals. The inductor that weakly couples in the magnetic flux from the DC current bias has an inductance much smaller than other sources of inductance.

tive inductance of the non-Foster device is

$$\begin{aligned} L_{\text{eff}} &= L_1 \left( 1 - \frac{k^2 L_2}{L_2 + L_J} \right) \\ &= L_1 \left( 1 - \frac{k^2 L_2}{L_2 + L_{J,0}/\cos\phi} \right). \end{aligned} \quad (5)$$

To ensure that the phase remains biased to a negative inductance value, we consider what the Josephson junction views as its “geometric inductance.” Generalizing the total matching network as series and parallel inductances across the input nodes of the junction yields the following expression:

$$L_G = L_2 \left( 1 - \frac{k^2 L_1}{L_1 + L_0} \right). \quad (6)$$

Here  $L_0$  is any upstream inductance that is not directly present within the non-Foster device loop. In our case, this is the “pickup” associated with the coupling of our signal source to our network, which is the source of impedance we want to match to achieve broadband power transfer.

Having obtained an expression for  $L_G$ , we refer back to Eq. 4 to calculate  $\phi$ . For the simple case where  $L_G < L_{J,0}$ ,  $\phi = \pi$  when the initial phase bias  $\phi_0 = \pi$ . This makes  $L_J$  negative, and if  $L_2 + L_J > 0$ ,  $L_{\text{eff}}$  will be negative for certain values of  $k$  and  $L_2$ , especially if  $k$  is sufficiently large or  $L_{J,0} \lesssim L_2$ .

Eq. 6 will be a consideration throughout the subsequent section, where  $L_G$  will be split into multiple inductors through configurations where they are in series, in parallel, or mutually inductive. Despite the expansion of the circuit, we maintain the final phase of the Josephson junction and control this in a way such that there is net effective inductance  $L_{\text{eff}}$  that cancels the reactive

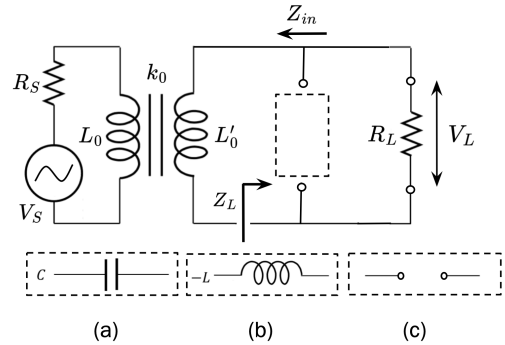


FIG. 5: Full signal model and matching network. Simulations are performed to compare three different impedance matching networks in a *pi*-network configuration: (a) classical capacitor match, (b) negative inductance match with the device proposed in Fig. 4, and (c) no match. The output voltage and subsequent power is measured across a  $50 \Omega$  load resistor  $R_L$ .

impedance  $L_0$  of the rest of the network. In the calculation of  $L_G$ , we do not consider any resistance in the network. Any resistance in the circuit could lead to runaway phase behavior in the junction, and even if the phase is biased to  $\pi$  the phase will slip to a different value which no longer cancels geometric inductance. This leads to a challenge in maintaining stability in the circuit, which will be considered afterwards.

### III. SIMULATION

From the results of Sec. IIB, we construct a circuit that uses the non-Foster component for impedance matching and simulate this using WRSPICE. WRSPICE is a circuit simulation tool based on LTSPICE which supports a variety of Josephson junction models<sup>39</sup>. In this work, we use a WRSPICE model based on the default RSCJ model<sup>40</sup>, which uses a capacitance of 0.7 nF per critical current in amperes. Simulated voltages, currents, and phases are obtained in the time domain. Using this data, the input power and output power of the circuit is calculated, and the ratio between the two will be taken as the value for power transfer. We compare this to impedance matching using a capacitor, as well as to a circuit where there is no matching component at all. In terms of axion experiments, the former are analogous to resonant experiments such as DMRadio and ADMX, and the latter to ABRACADABRA<sup>41–43</sup>.

All circuit types are constructed according to Fig. 5, then simulated with WRSPICE. In order to see the power transfer over a band of voltage source driving frequencies, we test the circuit using frequencies ranging from 30 MHz to 70 MHz, with a step size of 1 MHz. An individual simulation

was performed for each frequency, and the voltages and currents were measured at timescales past the initial transient behavior of the circuit. The input power was measured at the voltage source, and the output power was at the 50 ohm output resistor. The power in the input and output components of the circuit were calculated by obtaining the average power. Specifically, we took the product of the current and voltage, integrated this instantaneous power across multiple wavelengths, and then divided the integrated power by its time interval. The calculation of power using this method is equivalent to obtaining real power with the product of root-mean-square (rms) voltage, rms current, and the phase angle between the two quantities.

### A. Power Transfer Comparison Between Impedance Matching Circuits

The resonant circuit with a capacitor in parallel will be used as a passive, linear, and time invariant baseline for evaluating power transfer. In designing this circuit, the input resistance and output resistance were chosen to be 5 ohms and 50 ohms, respectively, and the quality factor is 500. The resonant frequency of the circuit was chosen to be 50 MHz, thus determining the values for  $L_0 = L'_0 = 3.183 \times 10^{-10}$  H, the coupling constant between them  $k_0 = 0.316$ , and the capacitor  $C = 3.183 \times 10^{-8}$  H. While the input inductance is split between two mutually inductive inductors ( $L_0$  and  $L'_0$ ), the relatively large value of  $R_S$  make the effective input inductance equal to  $L_0 = L'_0$ , which keeps the use of Eq. 6 consistent. The inductances were deliberately chosen to have  $\mathcal{O}(10^{-10})$  H values in consideration of typical Josephson junction inductances at critical currents around 1  $\mu$ A. Circuits with higher  $Q$  values, for example, could have been chosen, but this would change the input resistance value, assuming the output to be fixed at 50 ohms and the inductances in the circuit to maintain similar values. For this work, we chose a relatively lower  $Q$  and high input resistance to reduce the timescales for simulations to reach steady state behavior.

The second matching circuit uses a non-Foster matching network shown in Fig. 4. The effective contribution of the non-Foster component must have the same impedance as the capacitor in the resonant circuit. There are many combinations of  $L_1$ ,  $L_2$ , and  $k$  that satisfy Eq. 5 and produce a negative  $L_{\text{eff}}$  which gives the required impedance matching of the circuit. In this work, we use a combination with  $L_1 = 3.297 \times 10^{-10}$  H,  $L_2 = 3.449 \times 10^{-10}$  H, and  $k = 0.3$ . With a higher  $k$ , better power transfer can be achieved, but was set to 0.3 as a reasonable value that could be achievable during circuit fabrication.  $L_1$  and  $L_2$  were designed to be similar values and opti-

mized to produce the highest power transfer. The Josephson junction is set to have a critical current of 1  $\mu$ A, which corresponds to an inductance of  $3.291 \times 10^{-10}$  H when biased to zero phase. Assuming the Josephson junction settles at phase  $\pi$ , the effective inductance  $L_{\text{eff}}$  is equal to  $-3.183 \times 10^{-10}$  H, which is a negative value that cancels the input reactive impedance in the network.

The Josephson junction in the circuit can be biased to an intended initial phase, which was set to  $\pi$  for this set of simulations. While the initial phase can be directly set on the junction through WRSPICE, we instead inserted a small inductor into the loop with the junction that couples in magnetic flux to mimic a bias line in a fabricated chip. This additional inductor is inductively coupled to a separate loop which has a constant DC current which becomes the bias current for the junction. Its inductance is  $10^{-14}$  H, and has minimal effect on the total inductance of the circuit.

As an example, we present the difference in simulation results of the current and voltage across  $L_1$  when the junction phase has zero bias and when it is initially biased to  $\pi$ , shown in Fig. 6. Both simulations use a 50 MHz AC voltage source, with a voltage amplitude of  $10^{-10}$  V. The change in the voltage's phase relative to that of the current signifies that the sign of the inductance in the two simulations are opposite. In other words,  $L_{\text{eff}}$  is negative in the case where the Josephson junction is phase biased to  $\pi$ . This provides an impedance match similar to the capacitor in that it can cancel out reactive impedance in the rest of the circuit, but can also do so for a wider range of frequencies as the frequency dependence of pickup inductance in the circuit and  $L_{\text{eff}}$  from the matching network are identical.

Finally, the circuit is simulated without any matching component. In comparison to the resonant circuit, this circuit fully removes the parallel matching branch of the capacitor. The transfer of power is fully dependent on inductive reactance that has not been canceled, and therefore we expect its efficiency to suffer greatly.

Fig. 7 shows the power transfer between all three circuits. For the capacitively matched network (blue line), the power transferred to the output resistor shows the characteristics of a resonant circuit, with a quality factor of 500. When the input and output resistors are impedance matched at the resonance frequency of 50 MHz half of the power produced by the voltage source is dissipated by the output resistor. As a result, we see 3 dB loss on resonance between the input and output. The power transfer of the non-Foster network is shown in the green line in Fig. 7. Similarly to the resonant circuit, the average power is calculated at a time scale after the initial behavior that is caused by the Josephson junction in the circuit. In particular, we look at the power transfer at the  $\mu$ s scale, from 1  $\mu$ s to 2  $\mu$ s. The stability of this cir-

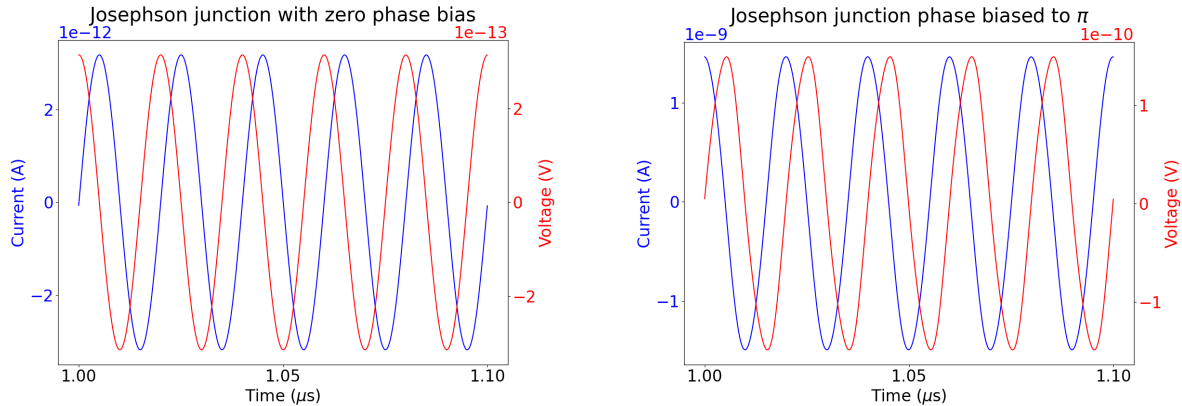


FIG. 6: Time domain simulation results in the non-Foster matching circuit when the Josephson junction's phase is initially biased to zero (left) and  $\pi$  (right). The current (blue) and voltage (red) across  $L_1$  are shown for each simulation. In the case where there is zero phase bias, the current lags behind the voltage, behaving like a normal inductor. This indicates that  $L_{\text{eff}}$  is positive. On the other hand, when the junction is phase biased to  $\pi$ , the current leads the voltage. In this case,  $L_{\text{eff}}$  is negative, and the phase of the voltage has flipped 180 degrees compared to the above simulation. As the effective inductance cancels out the rest of the inductance in the circuit, we can achieve an impedance match. This is also evident as the amplitudes of both current and voltage are higher in the latter plot.

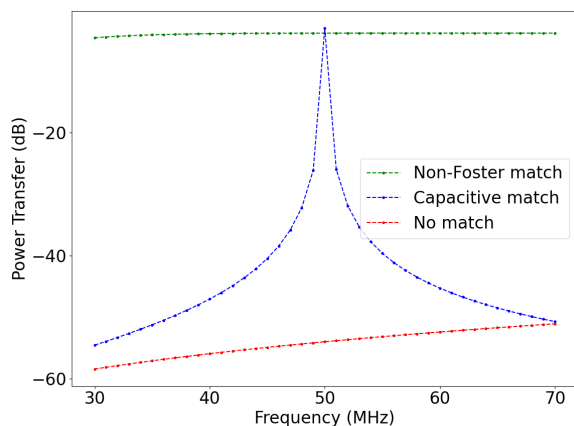


FIG. 7: The simulated power transfer comparison between a capacitively-matched resonant circuit (blue), a non-Foster impedance match circuit (green), and a circuit without any matching at all (red), from 30 MHz to 70 MHz. The resonance frequency of the resonant circuit is 50 MHz. Each point is a separate WRSPICE simulation done in the time domain, and power is calculated at a time scale after any initial, transient behavior in the circuit.

cuit, i.e., change in power transfer as a function of time, is discussed in the following subsection. For the time scales currently used, the power transfer is shown to be about -4 dB across the frequency range of interest, as shown in the green dotted line of Fig. 7. Overall, this shows that a broadband matching circuit can be achieved with the given non-Foster configuration with only a 1 dB differ-

ence from optimal transfer. The power transfer with no matching network is seen in the red line of Fig. 7. Since there is no impedance matching, the efficiency in power transfer is low. The non-Foster circuit power transfer, compared to this circuit, is better by about 50 dB.

As seen in the simulation results above, not only is the power transfer of the non-Foster circuit similar to that of a resonant impedance matching circuit, but it also exhibits an extended bandwidth. One consideration for the circuit is the power input and output of each type of circuit that was compared, shown in the top plot of Fig. 8. Due to the design of the circuit, the average power drawn by the voltage source decreases by roughly 50% at resonance for the resonant circuit. This decrease in power drawn by the voltage source can also be seen for the wider bandwidth of the non-Foster circuit, with values similar but slightly higher to the resonant circuit at resonance. Nevertheless, due to the high rates of power transfer, the total power that is dissipated by the output resistor is naturally higher when the impedance is matched (right plot of Fig. 8). While the resonant circuit does this for a small bandwidth of frequencies around 50 MHz, the non-Foster matching circuit can achieve a similar result with about 13% loss in output power from 30 MHz to 70 MHz.

Following the promising results from the non-Foster impedance matching circuit across 30 MHz to 70 MHz, an additional simulation was done to determine the full bandwidth for which the circuit maintains its impedance matching capabilities. In Fig. 9, the non-Foster circuit was simulated with WRSPICE for multiple orders of magnitude, from 10 MHz to 10 GHz. Simulations with higher volt-

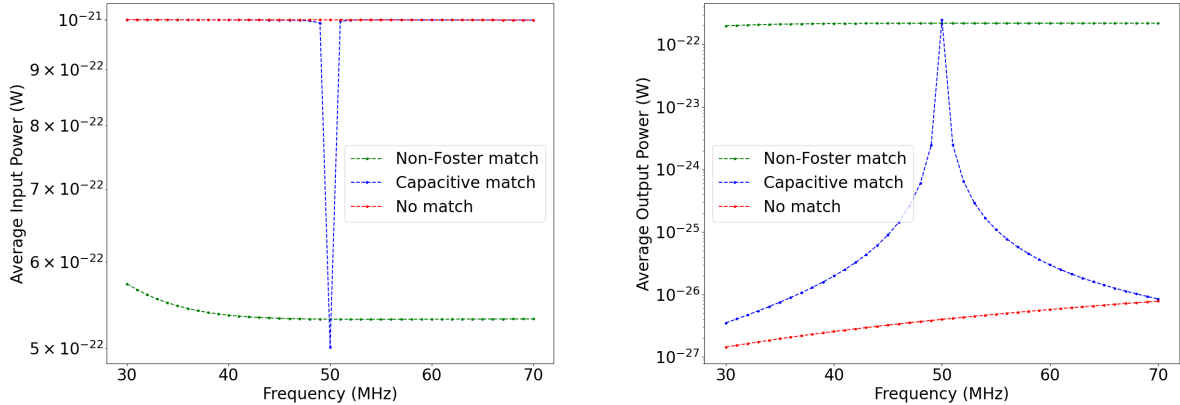


FIG. 8: Average input power (left) and output power (right) comparison between a capacitively-matched resonant circuit (blue), a non-Foster impedance match circuit (green), and a circuit without any matching at all (red), from 30 MHz to 70 MHz. The resonance frequency of the resonant circuit is 50 MHz. Each point is a separate WRSPICE simulation done in the time domain, and power is calculated at a time scale after any initial, transient behavior in the circuit. The input power is calculated at the voltage source, and the output power is calculated at the output resistor.

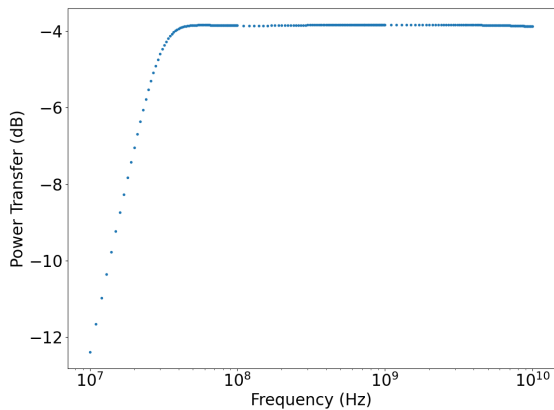


FIG. 9: The simulated power transfer of the previously described non-Foster impedance matching circuit. Simulations were done from 10 MHz to 10 GHz. Each point is a separate WRSPICE simulation done in the time domain, and power is calculated at a time scale after any initial, transient behavior in the circuit.

age source frequencies were not performed since the circuit model that was being used will no longer hold beginning with frequencies in the order of GHz. At these frequencies, additional considerations such as stray capacitance would be required for a more realistic simulation. Nevertheless, for the current set of simulations, the power transfer of the circuit is better than -4 dB from 30 MHz and onwards. This suggests that it is possible to maintain well-impedance-matched power transfer for arbitrarily high frequencies, provided that the circuit model used for the simulation is valid.

## B. Stability of the Non-Foster Circuit

In this subsection we will test the stability of the non-Foster impedance matching circuit formulated in the previous subsection. To do this, we first conduct the simulation for longer periods of time and see if the power transfer degrades over time. Another simulation will be the change in power transfer in the case where there is error in the bias current of the circuit. Both simulations give hints to the performance of the system under suboptimal conditions, such as when there is noise in the system.

Shown in Fig. 10 is the change in power transfer of the non-Foster impedance matching circuit with parameters used in Sec. III A. As time passes, the Josephson junction phase deviates further away from the initially intended phase  $\pi$ . After 1 ms, the power transfer drops to -12 dB from the -4 dB at 1  $\mu$ s. This result puts a constraint on the time duration of non-Foster circuit operation.

The second simulation, shown in Fig. 11, shows how the power transfer changes when there is error in the bias current. The fractional error in the bias current is proportional to the error in the initial phase bias for the Josephson junction, which is intended to be  $\pi$ . This simulation shows that the required accuracy of the bias current must be less than 100 parts per billion to maintain a similar level of power transfer from the optimal value. This result puts a constraint on the precision of bias current, which could be affected by noise.

Finally, we discuss the changes in power transfer when the inductor values on the non-Foster component change. This reflects fabrication conditions when the targeted inductance parameters are not perfectly produced. In Table I, we simulate the

Configuration	$L_1$	$L_2$	$k$	A	B	C
$L_{\text{eff}} = -L_0$	3.297	3.449	0.3	-3.844	-12.061	-30.625
$L_{\text{eff}} = -1.005L_0$	3.747	3.459	0.3	-8.035	-10.451	-30.154
$L_{\text{eff}} = -1.01L_0$	3.498	3.453	0.3	-13.331	-13.797	-29.615

TABLE I: Power transfer simulation results for three configurations of the non-Foster impedance matching circuit. The  $L_1$  and  $L_2$  values, whose inductances are in units of  $10^{-10}$  H, are varied. Based on the values of  $L_1$ ,  $L_2$ , and  $k$ , each configuration has an effective inductance  $L_{\text{eff}}$  equal to  $-L_0$ ,  $-1.005L_0$ , and  $-1.01L_0$ , respectively. For each configuration, three power transfer results, all in units of dB, are considered. The configurations are as follows. A: power transfer at 1  $\mu\text{s}$ , B: power transfer at 1 ms, C: power transfer at 1  $\mu\text{s}$ , with  $10^{-5}$  fractional error in bias current. For all configurations, the drive frequency of the voltage source is 50 MHz.

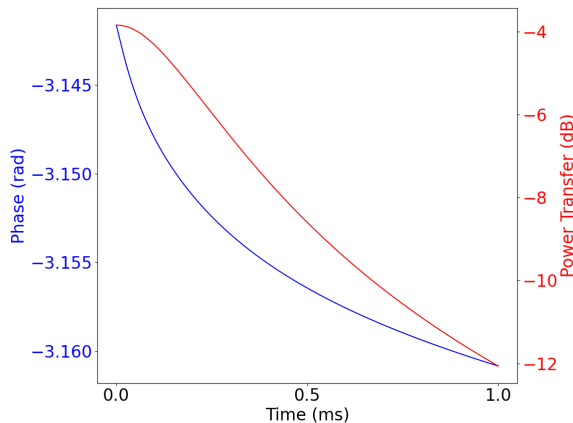


FIG. 10: The change in Josephson junction phase and power transfer as a function of time for the non-Foster impedance matching circuit with parameters used in Sec. III A. The input voltage source has a frequency of 50 MHz, and the simulation was done until 1 ms, as opposed to the  $\mu\text{s}$  scale simulation in the previous subsection. The initial behavior of the Josephson junction is removed for clarity.

non-Foster impedance matching circuit with similar values of  $L_1$  and  $L_2$ . The change in inductances will have  $L_{\text{eff}}$  that does not fully match the reactive inductance in the rest of the circuit. Due to this, the power transfer is lower. There is, however, an advantage in power transfer at longer scales as the dropoff in phase is slower, showing a more stable circuit. This observation suggests that there is a tradeoff between high power transfer and the duration of which this lasts. Power transfer loss due to bias current imprecision, on the other hand, remains relatively similar when the fractional error is  $10^{-5}$ . Due to this, maintaining a stable bias current with low fluctuations is expected to be an important task in practice.

The issues of stability in power transfer could be solved with a *time-variant* implementation of the bias current. In WRSPICE, the initial junction inductance can be re-established through the use

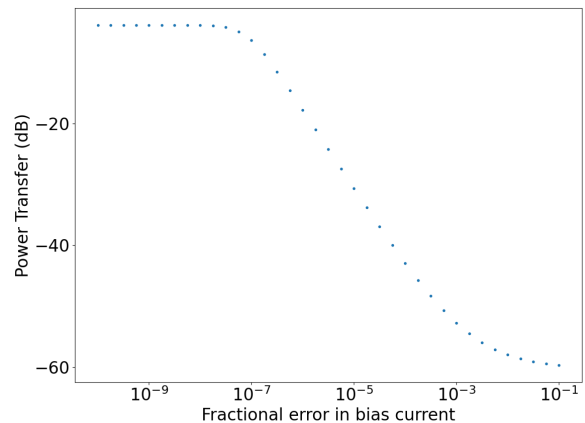


FIG. 11: Power transfer as a function of the error in bias current from its optimal point. Power transfer values were taken from time scales of 1  $\mu\text{s}$ . The power transfer begins to drop from the optimum value as the fractional error approaches  $10^{-7}$ .

of a periodic current pulse in the opposite direction. By alternating the sign of the bias current, the junction phase alternates between  $\pi$  and  $-\pi$ , which provide the same value for the inductance. Fig. 12 shows the results of such periodic pulsing of the bias current. The bias current changes sign every  $\mu\text{A}$  second, or every 25 wavelengths for the voltage source frequency (50 MHz). In contrast to a constant bias current, the phase of the Josephson junction remains at  $\pi$  (or  $-\pi$ ) up to the 1 ms scale when the bias current is pulsed. The output voltage for both simulations, shown in the bottom plot, also suggests that a pulsed bias current keeps the level of output steady up to at least 1 ms. By removing the data taken when there are spikes in voltage, which corresponds to when the sign of the bias current switches, it would be possible to sustain high power transfer for longer periods of time.

It is also possible to change the pulse duration to maintain a longer, coherent waveform, before the loss in power transfer degrades to a significant level. This optimization will depend on the

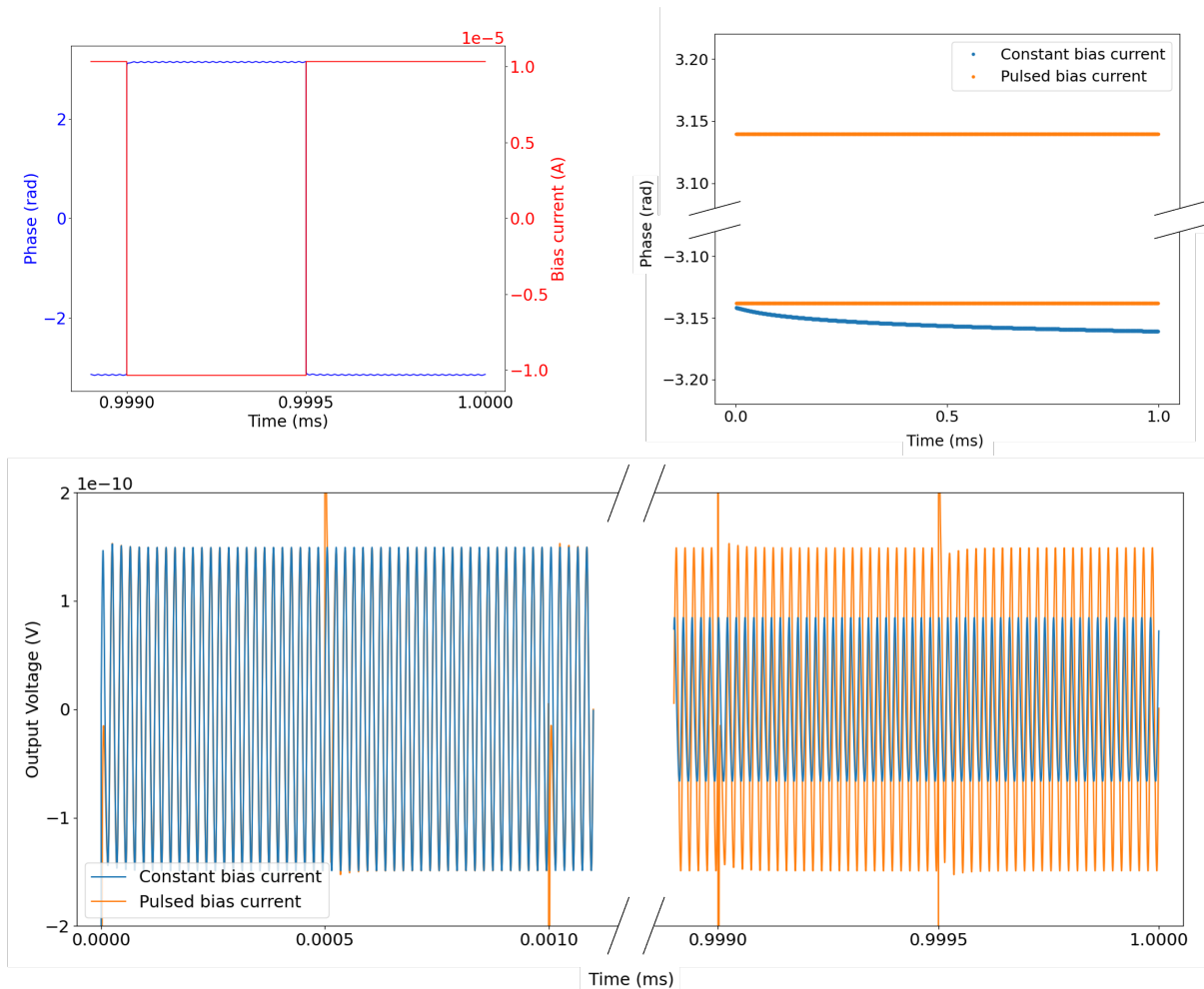


FIG. 12: Top left: A pulsed bias current and corresponding Josephson junction phase for a time domain WRSPICE simulation of the non-Foster impedance matching circuit. All parameters are the same as those used in the optimal power transfer simulation, except for the bias current, which changes sign every every  $0.5 \mu\text{A}$ . Only the last part of the simulation is shown. The voltage source frequency is  $50 \text{ MHz}$ , so each change in the bias current sign happens every 25 wavelengths. Top right: A comparison of the phase of the Josephson junction is shown for both constant and pulsed. Phase is averaged across every  $0.5 \mu\text{A}$ , equal to the duration of which the pulsed bias current remains at one value. The Josephson junction's phase under a pulsed bias current is either around  $\pi$  or  $-\pi$ , without showing any long term change in phase. The prevention of phase decay is not possible in the constant bias current simulation. Bottom: The output voltage for constant and pulsed bias current simulations. The beginning of the simulation and the end of the simulation are shown. The spikes in the pulsed bias current simulation correspond to each “pulse” where the bias current changes sign.

needs of each experiment that uses the non-Foster impedance matching circuit with a pulsed bias current.

#### IV. APPLICATION TO AXION SEARCHES

The rate of coverage of the axion parameter space, also known as the scan rate, depends on the model of the detector. Currently, axion searches below a few hundred MHz use lumped-element circuit models, similar to what has been described in prior sections. Above a few hundred MHz, it be-

comes difficult to use a lumped-element circuit, as stray inductance in the circuit will lower the resonant frequency. This barrier necessitates a different detector model at higher frequencies, motivating a transition to microwave cavities. An interesting aspect of the proposed circuit design is that inductance cancellation could remove or shift the existing delineations between detector models within the axion frequency space.

Among cavity searches, a separate issue further impedes the scan rate. The simplest resonator that will fit in a solenoidal magnet bore is a right cylindrical cavity, whose volume,  $V$ , scales with frequency,  $\nu$ , as  $\nu^{-3}$ . Accounting for the frequency

scaling of the quality factor ( $Q \sim \nu^{-2/3}$ ), the scan rate scales as  $\nu^{-14/3}$ . This precipitous decline in the scan rate at higher frequencies is one of the largest challenges in the field, and compounds the issue of the Bode-Fano limits on passive matching networks that exists across all frequencies<sup>33</sup>. The technique proposed here may be applicable in this regime, but a different circuit model is needed to fully evaluate the efficacy of the concept at frequencies above a GHz.

A complete understanding of the possible axion scan rate cannot be made without a full accounting of the noise in any detector. Through the Dicke-Radiometer equation, the total system noise,  $T_{\text{sys}}$ , and the integration time,  $t$ , are related to the signal-to-noise (SNR) through  $\text{SNR} \propto \sqrt{t}/T_{\text{sys}}$ . Active components, and therefore non-Foster circuits, necessarily contribute more to the total system noise. For biased Josephson junctions operating in nonlinear regimes, the utility of a quantitative noise model is limited without an experimental realization. A few possible noise mechanisms include critical current fluctuations, quasiparticle-related noise, bias current noise coupling into junction phase fluctuations, and conversion of phase noise into amplitude noise when operating near  $\phi \approx \pi$ . A complete understanding of the noise requires a dedicated measurement of the signal-to-noise improvement with and without the non-Foster component.

While a precise accounting of the noise is not possible without a prototype, we can make a very rough approximation of the impact on the SNR. In a typical axion search, the detector consists of the resonator read out by a low noise quantum amplifier. Since our device leverages the Josephson junction, which is a fundamental building block of these quantum amplifiers, one could assume there is added noise in the resonator at the level of a typical quantum amplifier, such as a SQUID. Since the total system noise is additive, this essentially doubles the amplifier noise associated with existing axion detectors. All else held equal, including the instantaneous bandwidth of the detector, if it takes time  $\tau$  to achieve a given SNR with a passive capacitive matching circuit, then, assuming a doubling of the noise, a non-Foster circuit will take time  $4\tau$  to achieve the same sensitivity.

Our results suggest a possible increase in the instantaneous bandwidth by a factor of  $\sim 1,000$ . If we assume a doubling of the amplifier noise (and a factor of four increase to the required integration time), the scan rate would then increase by a factor of  $\sim 250$ . Furthermore, the proposed technique eliminates the need for slow and complex mechanical tuning mechanisms that frequently jam and, through frictional heating, raise the base temperature of the cryostat. Nevertheless, a thorough study of the added noise in a variety of implementations and real lab conditions, is critical to

assessing the benefit to axion searches.

An interesting aspect of this approach is that the broadband capabilities of the readout necessarily entail faster signal processing. Data acquisition could become a bottleneck in the absence of thorough consideration. Fortunately, digital signal processing has made great strides in recent decades. At high frequencies, this endeavor could stand to benefit from high-speed, high-throughput Radio Frequency System on a Chip (RFSoc) systems with sampling rates as high as 10 GSPS. The telecommunications industry has driven the advancement of these systems to allow for rapid gains in the speed of digital signal processing. The consolidation of various controls and data acquisition instrumentation onto a single RFSoc would provide the ability to tightly synchronize the feedback controls necessary for junction rebiasing with the data-taking operation. We propose that, through the use of an automated rebiasing scheme that provides a fixed duty cycle, axion data could be acquired in the intervals between pulses and co-added via standard analysis procedures offline. Operations under these conditions would require a robust understanding of the repeatability and rate of phase roll-off for the duration of an experimental measurement.

## V. CONCLUSION

In conclusion, we present a conceptual design for a Josephson junction operated as a non-Foster circuit component. We believe this circuit represents one possible solution to the longstanding scan rate problem facing axion searches, with a potential increase to the instantaneous bandwidth by a factor of  $\sim 1,000$ . To further evaluate the efficacy of this technique, we propose to fabricate the non-Foster circuit on a chip and demonstrate the power sourced and transferred from the AC input as shown here. Of particular importance is a robust characterization of the circuit noise and stability. Mitigation of instability, through the application of a controlled pulse signal, may be one step towards the implementation of this technique in an axion experiment. We note that, though challenging, the stability issue may represent a more readily solvable problem than those currently impeding the scan rate of existing searches. Finally, low-noise, broadband detection of electromagnetic signals is relevant to a variety of fields, such as astronomy, nuclear, and condensed matter physics, especially in the context of spectroscopy<sup>44–46</sup>. As such, we believe this approach may find other applications beyond the more immediate implementation in the detection of axion dark matter.

## VI. ACKNOWLEDGEMENTS

The authors are extremely grateful to the DM-Radio and ADMX collaborations for thoughtful conversation and feedback on the manuscript. They also extend thanks to David Schuster and Noah Kurinsky for their insightful commentary on quantum techniques and device physics.

Chelsea Bartram, Andrew Yi and the conceptual idea, design and simulations presented in this work were supported by the Department of Energy, Laboratory Directed Research and Development program at SLAC National Accelerator Laboratory, under contract DE-AC02-76SF00515 and as part of the Panofsky Fellowship awarded to Chelsea Bartram. Pamela Stark is supported by the National Science Foundation Graduate Research Fellowship under Grant No. DGE-2146755.

## AUTHOR DECLARATIONS

The authors have no conflicts to disclose.

## DATA AVAILABILITY STATEMENT

The data that support the findings of this study are available from the corresponding author upon reasonable request.

- <sup>1</sup>D. M. Pozar, *Microwave engineering: theory and techniques* (John Wiley & Sons, 2021).
- <sup>2</sup>W.-K. Chen, *Broadband matching: Theory and implementations*, Vol. 18 (World Scientific, 2015).
- <sup>3</sup>R. E. Collin, *Foundations for microwave engineering* (John Wiley & Sons, 2007).
- <sup>4</sup>R. M. Fano, "Theoretical limitations on the broadband matching of arbitrary impedances," *Journal of the Franklin Institute* **249**, 57–83 (1950).
- <sup>5</sup>H. W. Bode, *Network analysis and feedback amplifier design* (D. Van Nostrand Company, Inc., 1945).
- <sup>6</sup>R. M. Foster, "A reactance theorem," *The Bell System Technical Journal* **3**, 259–267 (1924).
- <sup>7</sup>S. Hrabar, I. Krois, A. Brizic, D. Zanic, K. Lebo, D. Nozina, and B. Okorn, "Non-foster networks for tunable and wideband rf devices," *Tech. Rep. AFRL-AFOSR-UK-TR-2023-0060* (Air Force Office of Scientific Research, 2023).
- <sup>8</sup>J. Merrill Jr, "Theory of the negative impedance converter," *Bell System Technical Journal* **30**, 88–109 (1951).
- <sup>9</sup>A. Larky, "Negative-impedance converters," *IRE Transactions on Circuit Theory* **4**, 124–131 (1957).
- <sup>10</sup>E. Yuce, "Negative impedance converter with reduced nonideal gain and parasitic impedance effects," *IEEE Transactions on Circuits and Systems I: Regular Papers* **55**, 276–283 (2008).
- <sup>11</sup>Y. Ren, D. Huang, B. Feng, Q. Ren, H. Hu, and J. Zhou, "A high gain, compact active disc-cone antenna based on non-foster matching circuit," *AEU - International Journal of Electronics and Communications* **133**, 153644 (2021).
- <sup>12</sup>M. M. Jacob, J. Long, and D. F. Sievenpiper, "Broadband non-Foster matching of an electrically small loop antenna," in *Proceedings of the 2012 IEEE International Symposium on Antennas and Propagation* (IEEE) pp. 1–2.
- <sup>13</sup>P. Lohmannia and M. Manteghi, "Broadband Parametric Impedance Matching for Small Antennas Using the Bode-Fano Limit: Improving on Chu's limit for loaded small antennas," *IEEE Antennas and Propagation Magazine* **64**, 55–68 (2022).
- <sup>14</sup>S. E. Sussman-Fort and R. M. Rudish, "Non-Foster impedance matching of electrically-small antennas," *IEEE Transactions on Antennas and Propagation* **57**, 2230–2241 (2009).
- <sup>15</sup>A. Mekawy, H. Li, Y. Radi, and A. Alù, "Parametric enhancement of radiation from electrically small antennas," *Physical Review Applied* **15**, 054063 (2021).
- <sup>16</sup>S. A. Tretyakov and T. G. Kharina, "The perfectly matched layer as a synthetic material with active inclusions," *Electromagnetics* **20**, 155–166 (2000).
- <sup>17</sup>S. Hrabar, I. Krois, and A. Kirichenko, "Towards active dispersionless ENZ metamaterial for cloaking applications," *Metamaterials* **4**, 89–97 (2010).
- <sup>18</sup>S. Hrabar, "First ten years of active metamaterial structures with "negative" elements," *EPJ Applied Metamaterials* **5**, 9 (2018).
- <sup>19</sup>M. M. Jacob and D. F. Sievenpiper, "Non-foster matched antennas for high-power applications," *IEEE Transactions on Antennas and Propagation* **65**, 4461–4469 (2017).
- <sup>20</sup>J. Long and D. F. Sievenpiper, "Stable multiple non-Foster circuits loaded waveguide for broadband non-dispersive fast-wave propagation," *Electronics Letters* **50**, 1708–1710 (2014).
- <sup>21</sup>J. Long, M. M. Jacob, and D. F. Sievenpiper, "Broadband fast-wave propagation in a non-Foster circuit loaded waveguide," *IEEE Transactions on Microwave Theory and Techniques* **62**, 789–798 (2014).
- <sup>22</sup>D. F. Sievenpiper, "Superluminal waveguides based on non-Foster circuits for broadband leaky-wave antennas," *IEEE Antennas and Wireless Propagation Letters* **10**, 231–234 (2011).
- <sup>23</sup>P. Sikivie, "Experimental tests of the "invisible" axion," *Physical Review Letters* **51**, 1415 (1983).
- <sup>24</sup>R. D. Peccei and H. R. Quinn, "CP conservation in the presence of pseudoparticles," *Phys. Rev. Lett.* **38**, 1440–1443 (1977).
- <sup>25</sup>F. Wilczek, "Problem of Strong p and t Invariance in the Presence of Instantons," *Phys. Rev. Lett.* **40**, 279–282 (1978).
- <sup>26</sup>S. Weinberg, "A New Light Boson?" *Phys. Rev. Lett.* **40**, 223–226 (1978).
- <sup>27</sup>M. Dine, P. Draper, L. Stephenson-Haskins, and D. Xu, "Axions, instantons, and the lattice," *Phys. Rev. D* **96**, 095001 (2017).
- <sup>28</sup>M. Dine, W. Fischler, and M. Srednicki, "A Simple Solution to the Strong CP Problem with a Harmless Axion," *Phys. Lett.* **B104**, 199 (1981).
- <sup>29</sup>A. Zhitnitsky, "On Possible Suppression of the Axion Hadron Interactions. (In Russian)," *Sov. J. Nucl. Phys.* **31**, 260 (1980).
- <sup>30</sup>M. Dine and W. Fischler, "The not-so-harmless axion," *Physics Letters B* **120**, 137–141 (1983).
- <sup>31</sup>S. J. Asztalos, G. Carosi, C. Hagmann, D. Kinion, K. Van Bibber, M. Hotz, L. Rosenberg, G. Rybka, J. Hoskins, J. Hwang, *et al.*, "Squid-based microwave cavity search for dark-matter axions," *Physical review letters* **104**, 041301 (2010).
- <sup>32</sup>N. Du, N. Force, R. Khatiwada, E. Lentz, R. Ottens, L. Rosenberg, G. Rybka, G. Carosi, N. Woollett, D. Bowring, *et al.*, "Search for invisible axion dark matter with the axion dark matter experiment," *Physical review letters* **120**, 151301 (2018).
- <sup>33</sup>M. Malnou, D. Palken, B. Brubaker, L. R. Vale, G. C. Hilton, and K. Lehnert, "Squeezed vacuum used to accelerate the search for a weak classical signal," *Physical Review X* **9**, 021023 (2019).

- <sup>34</sup>S. Chaudhuri, K. Irwin, P. W. Graham, and J. Mardon, “Optimal impedance matching and quantum limits of electromagnetic axion and hidden-photon dark matter searches,” arXiv preprint, arXiv:1803.01627 (2018).
- <sup>35</sup>S. Chaudhuri, “Impedance matching to axion dark matter: considerations of the photon-electron interaction,” *Journal of Cosmology and Astroparticle Physics* **2021**, 033 (2021).
- <sup>36</sup>R. Rifkin and B. S. Deaver Jr, “Current-phase relation and phase-dependent conductance of superconducting point contacts from rf impedance measurements,” *Physical Review B* **13**, 3894 (1976).
- <sup>37</sup>J. M. Martinis, “Superconducting qubits and the physics of josephson junctions,” in *Les Houches*, Vol. 79 (Elsevier, 2004) pp. 487–520.
- <sup>38</sup>J. Clarke and A. I. Braginski, *The SQUID handbook: Applications of SQUIDs and SQUID systems* (John Wiley & Sons, 2006).
- <sup>39</sup>Whiteley Research Inc., “WRSPICE Circuit Simulator,” (2024).
- <sup>40</sup>R. E. Jewett, “Josephson Junctions in SPICE2G5,” ERL Memo, Electronics Research Laboratory, University of California, Berkeley (1982).
- <sup>41</sup>A. AlShirawi, V. Ankel, C. Bartram, J. Begin, C. Bell, J. Benabou, L. Brouwer, S. Chaudhuri, H.-M. Cho, J. Corbin, *et al.*, “Electromagnetic modeling and science reach of DMRadio-m<sup>3</sup>,” *Physical Review D* **112**, 052001 (2025).
- <sup>42</sup>L. J. Rosenberg and E. J. Daw, *A search for halo axions*, Ph.D. thesis, Massachusetts Institute of Technology (1998).
- <sup>43</sup>C. P. Salemi, J. W. Foster, J. L. Ouellet, A. Gavin, K. M. Pappas, S. Cheng, K. A. Richardson, R. Henning, Y. Kahn, R. Nguyen, *et al.*, “Search for low-mass axion dark matter with ABRACADABRA-10 cm,” *Physical review letters* **127**, 081801 (2021).
- <sup>44</sup>J. Formaggio, Project 8 Collaboration, *et al.*, “Project 8: using radio-frequency techniques to measure neutrino mass,” *Nuclear Physics B-Proceedings Supplements* **229**, 371–375 (2012).
- <sup>45</sup>Z. Ji, M. E. Barber, Z. Zhu, C. R. Kometter, J. Yu, K. Watanabe, T. Taniguchi, M. Liu, T. P. Devereaux, B. E. Feldman, *et al.*, “Local microwave sensing of excitons and their electrical environment,” *Nature Communications* **16**, 9236 (2025).
- <sup>46</sup>D. Aybas, H. Bekker, J. W. Blanchard, D. Budker, G. P. Centers, N. L. Figueroa, A. V. Gramolin, D. F. Jackson Kimball, A. Wickenbrock, and A. O. Sushkov, “Quantum sensitivity limits of nuclear magnetic resonance experiments searching for new fundamental physics,” *Quantum Science & Technology* **6**, 034007 (2021).